IEEE Access
Multidisciplinary ⋮ Rapid Review ⋮ Open Access Journal

Received 31 March 2023, accepted 10 May 2023, date of publication 15 May 2023, date of current version 24 May 2023.

Digital Object Identifier 10.1109/ACCESS.2023.3276239

RESEARCH ARTICLE

Project-Oriented RF Coil Comparison and Optimization for Preclinical, Single-Voxel MR Spectroscopy of the Rat Visual Cortex at 9.4 T

CHANG-HOON CHOI[1,*], EZEQUIEL FARRHER[1,*], JÖRG FELDER[1,2], (Senior Member, IEEE), JING WANG[1], ANTJE WILLUWEIT[1], AND N. JON SHAH[1,2,3,4,5]

[1]Institute of Neuroscience and Medicine—4, Forschungszentrum Juelich, 52428 Juelich, Germany
[2]RWTH Aachen University, 52062 Aachen, Germany
[3]Institute of Neuroscience and Medicine—11, JARA, Forschungszentrum Juelich, 52428 Juelich, Germany
[4]JARA—BRAIN—Translational Medicine, 52062 Aachen, Germany
[5]Department of Neurology, RWTH Aachen University, 52062 Aachen, Germany

Corresponding author: Chang-Hoon Choi (c.choi@fz-juelich.de)

*Chang-Hoon Choi and Ezequiel Farrher contributed equally to this work.

This work was supported by the Deutsche Forschungsgemeinschaft—DFG (German Research Foundation) under Grant 491111487.

This work involved human subjects or animals in its research. Approval of all ethical and experimental procedures and protocols was granted by the Animal Protection Committee of the Local Government (LANUV), North-Rhine-Westphalia, Germany, under Approval No. AZ 81-02.04.2021.A111.

ABSTRACT As one of the most important cortical structures in the brain, the visual cortex plays a primary role in processing visual data. Observing the metabolic changes in this region using single-voxel MR spectroscopy (MRS) can provide a plethora of information on the disease stage and progress *in vivo*. For single-voxel MRS experiments, a target voxel is always chosen and specifically investigated. The volume of the voxel must be sufficiently small to avoid any interference from adjacent areas but large enough to maximise its signal-to-noise ratio (SNR). Of the factors used to improve SNR, e.g. enlarging voxel size or increasing the number of signal averaging, the optimisation of the RF coil can contribute significantly to the SNR improvement. In this work, we compared and optimised RF coils which include a circularly-polarised (CP) high-pass birdcage coil and two CP surface coils with different dimensions. The coils were particularly designed for the entire rat head, brain and the target region (visual cortex), respectively. The performance of these coils was evaluated based on the project-specific purpose of investigating metabolite concentration changes in the visual cortex of the *in vivo* rat brain, assessed by means of single-voxel MRS at 9.4 T. In the SNR comparison, the values obtained using the optimised small loop coil were found to be approximately 5 and 1.35 times higher than those using the birdcage volume head coil and the medium-sized loop coil, respectively. In other words, using the optimised coil rather than, for example, the birdcage coil allows the acquisition to be completed more quickly by a factor of 25 times. In conclusion, by using the optimised setup, we can i) benefit either from reduced measurement time or in the acquisition of high-quality MR images or ii) obtain spectra with a minimum quantification error.

INDEX TERMS MRI, MRS, spectroscopy, coil, optimization, preclinical, small animal, single-voxel.

I. INTRODUCTION

Small animal models have become important tools for broadening our understanding of various complex disease processes [1], [2], [3] and for translational research [4], [5]. The visual cortex is one of the most important cortical structures in the brain and is primarily associated with the processing of visual information. Studies have revealed that eye disorders associated with retinal degeneration, including glaucoma [6], retinitis pigmentosa [7] and age-related

The associate editor coordinating the review of this manuscript and approving it for publication was Marco Giannelli.

macular degeneration [8], and systemic diseases, such as diabetes [9] and systemic lupus erythematosus [10] can trigger interactive structural and functional reorganisations of the visual cortex. The current therapeutic approaches for retinal degenerative diseases are limited and mainly aim to restore or substitute the retinal input. The latter, however, relies on the plasticity of the visual cortex, whereby visual cortical circuits are re-adapted after long-term deafferentation (following, in some cases, decades of blindness) [11]. Evaluation of the consequences of vision loss on the visual cortex may help us to understand the mechanisms involved in cortical rewiring and may help to support further ways to improve signal transduction along the visual pathway. In this respect, non-invasive imaging techniques, such as magnetic resonance imaging (MRI) or magnetic resonance spectroscopy (MRS), are valuable tools for studying the development of the structural and functional consequences of retinal visual field defects in the visual cortex over time.

Single-voxel proton (^{1}H) MRS is a well-established, non-invasive technique used to sensitively quantify the concentrations of diverse metabolites in the brain *in vivo* [12], [13]. For example, as primary regulators in the brain, glutamate (Glu) and γ-aminobutyric acid (GABA) play pivotal roles as neurotransmitters and are closely connected to physiological processes and neurological conditions [14]. Analysing changes in the concentration of these metabolites using MRS allows access to information that is complementary to anatomical MRI.

For MRS experiments, a target voxel or voxel-of-interest (VOI) is selected and precisely placed on a high-resolution anatomical MR image, typically obtained using longitudinal relaxation time weighted (T_1w) or transverse relaxation time weighted (T_2w) imaging. The volume of the VOI is usually chosen to be sufficiently small so as to avoid any signal contamination by the partial volume effect from adjacent regions but large enough in order to maximise its signal-to-noise ratio (SNR) [15]. Therefore, although voxel size selection is a trade-off requiring thoughtful adjustment, in most cases, a detectable signal level from a single acquisition is too low for reliable quantification. In order to compensate for this, the measurement tends to be repeated multiple times, thus leading to a prolonged total acquisition time.

Another crucial consideration in any MRS experiment is associated with the radiofrequency (RF) coil – an essential unit in the MRI machine that plays a crucial role in the transmission of RF power to the object and in receiving signals from it. At a given magnetic field strength, the quality of the MR image or spectrum and detection coverage are determined, to a great extent, by the choice of the RF coil. Thus, depending on the purpose of use, its dimensions and geometry should be optimised carefully. Most commercially available MR RF coils provided by the scanner or coil manufacturers tend to be universal rather than project-specific, which means that they are usually designed to cover an entire volume, such as either the whole head or whole body, with reasonable SNR and image quality. While this approach is generally useful for acquiring anatomical scout MR images with a large field-of-view, covering the entire area of an object is not necessary for most studies, which instead require a much higher image or spectrum quality of one target region. This prerequisite can be even more pronounced when performing, e.g. single-voxel MRS experiments. Generally, single-voxel MRS experiments just concentrate on acquiring data from a particularly small voxel, which is placed at a predetermined location of interest and it is not necessary to cover a large area (e.g. the whole brain).

In a given measurement time, the desired resolution is restricted by the SNR, which, in turn, is significantly determined by the choice of the RF coil. Thus, project-oriented optimisation of RF coils should offer the benefit of sizeable improvements in SNR. Fundamentally, the size of coil is inversely proportional to the SNR while being proportional to its coverage and penetration depth [16]. Consequently, the coil does not have to be gigantic, and a small coil should operate in an optimal manner which maximises the sensitivity for single-voxel MRS.

In this work, we designed and constructed three frequently-used RF coil configurations, namely a quadrature birdcage head coil, a circularly polarised (CP) medium-sized loop coil and a small CP loop coil. The performance of these coils was evaluated and compared based on the project-specific aim of characterising the metabolic profile of the visual cortex in the rat brain, assessed by means of single-voxel MRS.

II. METHODS

A. RF COILS

Since the (visual) cortex is closely located to the surface of the brain, it is possible to access the region using a highly sensitive surface coil. Three different CP coils were constructed and compared on the bench and on the scanner: one high-pass birdcage coil (with 42 mm inner diameter, 28 mm length, 5 mm width, 8 rungs) and two surface coils with different dimensions (medium loop: 9 mm × 15 mm and small loop: 9 mm × 6 mm). These were particularly optimised for the entire rat head, brain and the target region (visual cortex), respectively. The two medium-size and small-size surface coils were configured using a combination of two identical loops, which were carefully overlapped in order to isolate the B_1 fields from each loop in a geometrical decoupling manner [17]. Figure 1 shows pictures and circuit diagrams along with the dimensions and component values of the RF coils designed and used in this work. The scattering parameters of the coils were measured using a vector network analyser (ZNB4, Rohde & Schwarz, Germany) and were better than -15 dB when applied to the *in vivo* animal.

B. ANIMAL PREPARATION

One healthy female wild-type rat (strain RCS-rdy+p+/LavRrrc), six months old and weighing 220 g, was used for

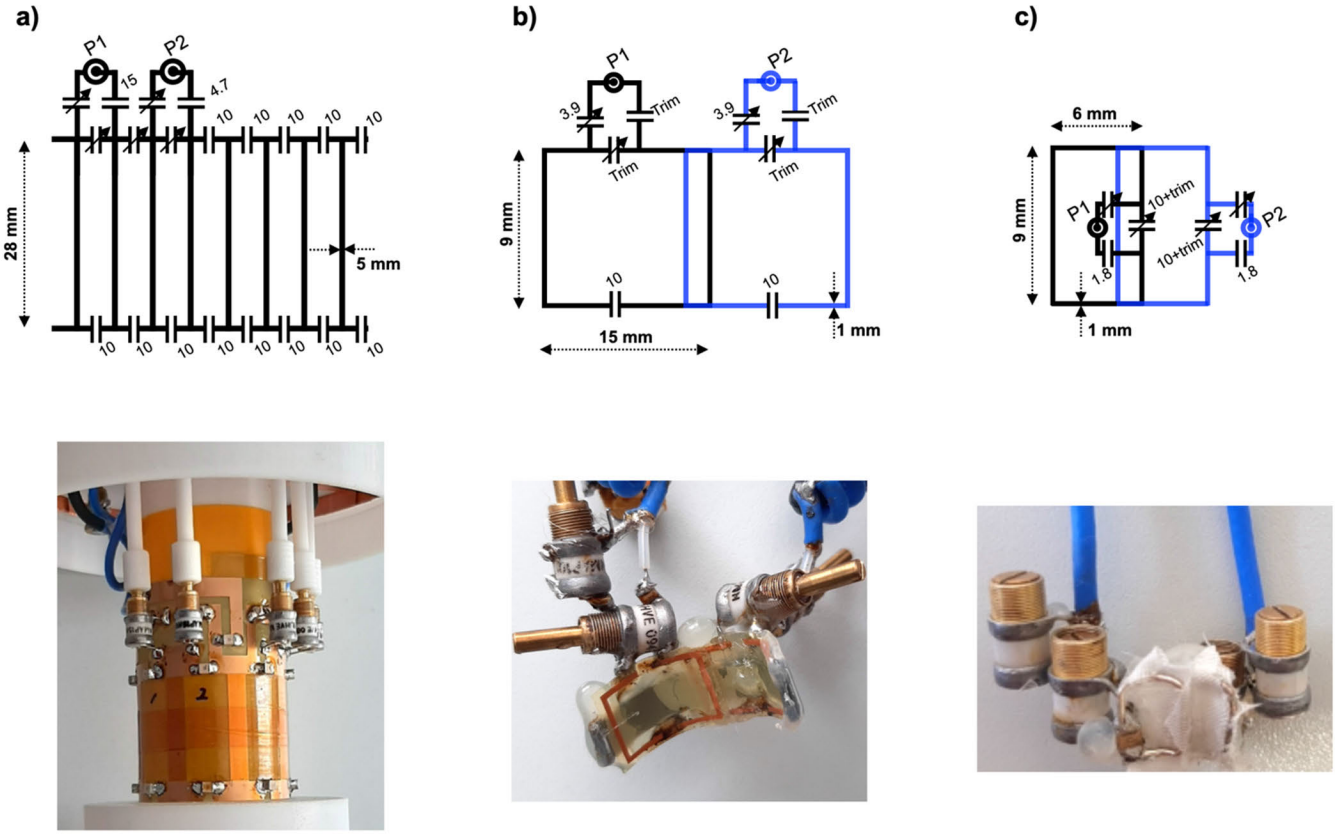

FIGURE 1. Schematic diagrams and pictures of the RF coils used in this study a) CP birdcage volume head coil, b) CP medium-sized brain loop coil and c) CP optimised small loop coil - including the dimensions and the values (unit: pF) of the capacitors. trim. refers to trimmer or variable capacitor and P1 and P2 refer to the port 1 and port 2 of each coil.

the in vivo MR measurement. The rat was bred in the animal facility at Forschungszentrum Jülich and was reared in a controlled environment with a 24 h light/dark cycle (12/12 h), 54% humidity, and a temperature of 22°C. Food and water were available *ad libitum*.

The animal study was approved by the Animal Protection Committee of the local government (LANUV, North-Rhine-Westphalia, Germany; AZ 81-02.04.2021.A111) and was performed in accordance with the German Law on the protection of animals, according to the German Animal Welfare Act and the European Community Council directives regarding the protection of animals used for experimental and scientific purposes (2010/63/EU). The rat was anaesthetised with 1.5 to 2.5% isoflurane inhalation via a nose cone and placed into the animal scanner. All animal measurements were conducted under continuous isoflurane anaesthesia. The temperature and respiratory rate of the rat were continuously maintained at around 37°C and between 50 to 65 breaths per minute, respectively.

C. MR EXPERIMENTS

All MR measurements were carried out on a home-integrated small animal dedicated 9.4 T MRI scanner operating on Siemens clinical software [18], [19]. T_2w images were acquired using the turbo spin-echo (TSE) sequence [20] and were used to precisely position the VOI in the visual cortex. The sequence was repeated three times with high in-plane resolution in the axial, coronal and sagittal slice orientations. The parameters for the TSE sequence were: repetition-time (TR) = 3030 ms; echo-time (TE) = 39 ms; in-plane resolution = 0.1 × 0.1 mm^2; slice thickness = 0.5 mm; number of averages = 2 and scan time = 2:27 minutes for each slice orientation.

Prior to the MRS acquisition, first- and second-order shimming at the VOI was performed using FASTESTMAP [21]. We repeatedly applied this until the full width at half maximum (FWHM) of the water spectrum was reached to approximately 30 Hz. Water suppression was achieved with the variable power and optimised relaxation delays (VAPOR) method [22], with the timings optimised for the voxel placed on the visual cortex. Using a variable flip angle method, the transmit power was calibrated within the VOI for each coil. All MR spectra were measured using the LASER sequence [23], [24], [25], with excitation performed using a nonselective numerically optimised adiabatic half-passage pulse and localisation performed with three pairs of adiabatic full passage pulses in each dimension (HS8, R15). Other important MRS parameters were: TR = 2500 ms;

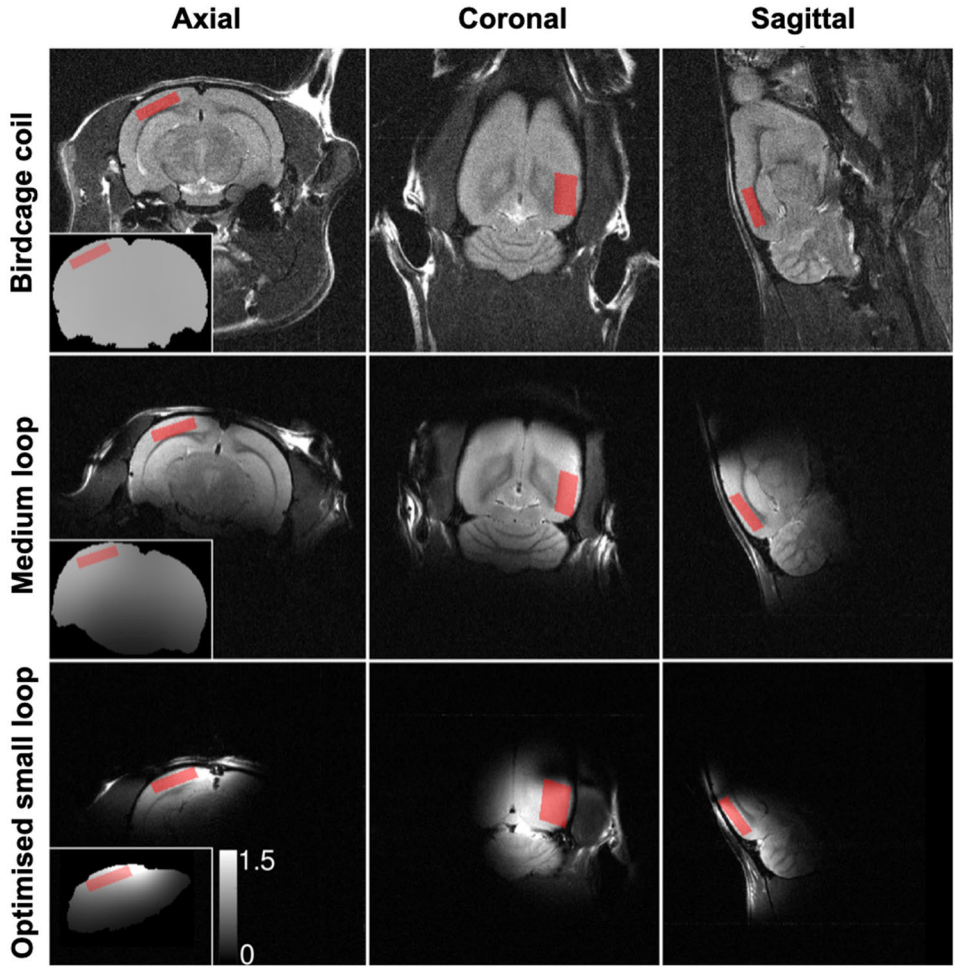

FIGURE 2. T_2w TSE MR images in three axes (axial, coronal and sagittal) obtained using the birdcage coil (top), medium-sized loop coil (middle) and optimised small loop coil (bottom). Their corresponding B_1 bias field maps are also shown in the bottom left corner in axial images. The images clearly display the coverage of each coil. The regions used to calculate SNRs are shown in red.

TE = 39 ms; number of averages = 512; voxel-size = 4 × 1 × 4 mm^3; receive-bandwidth, 4000 Hz; vector-size = 2048 and scan time = 22:20 minutes. One extra spectrum (eight repetitions) was obtained without the water suppression RF pulses for its use in eddy-current correction and quantification of the water suppressed spectrum.

D. MR DATA PROCESSING

The SNR values of the images were calculated using the equation of the signal intensity mean value (within the VOI – red area in Figure 2) divided by the standard deviation of the noise (left bottom corner). Furthermore, based on the T_2w images, the corresponding sequence-specific B_1 bias field maps of each coil in Figure 2 (bottom left corner) were estimated using the tool 'fast' available in the FSL software package [26].

All spectra were pre-processed using MATLAB with the aid of the FID-A package [27]. The pre-processing steps included i) automatic detection and removal of motion-corrupted scans and ii) phase and frequency drift correction of individual transients [28]. Note that due to the intrinsically low SNR of each individual transient, spectra were first averaged in groups of 16 before pre-processing steps i) and ii) were performed. Quantification of the pre-processed data was performed using LCModel software [29] with the water scaling and eddy current correction options enabled. Fitting was performed in the chemical shift range of 0.2 ppm to 4.2 ppm. The metabolite basis sets were generated by means of the FID-A package using the density matrix formalism [30] with ideal RF pulses and actual sequence timings [31], [32]. The basis set included spectra of 19 metabolites, namely alanine (Ala), ascorbate (Asc), aspartate (Asp), creatine (Cr), GABA, glucose (Glc), glutamine (Gln), Glu, glutathione (GSH), glycerophosphorylcholine (GPC), *myo*-inositol (Ins), lactate (Lac), N-Acetylaspartic acid (NAA), N-acetylaspartylglutamate (NAAG), phosphocreatine (PCr), phosphorylcholine (PCh), phosphorylethanolamine (PE), *scyllo*-inositol (Scyllo),

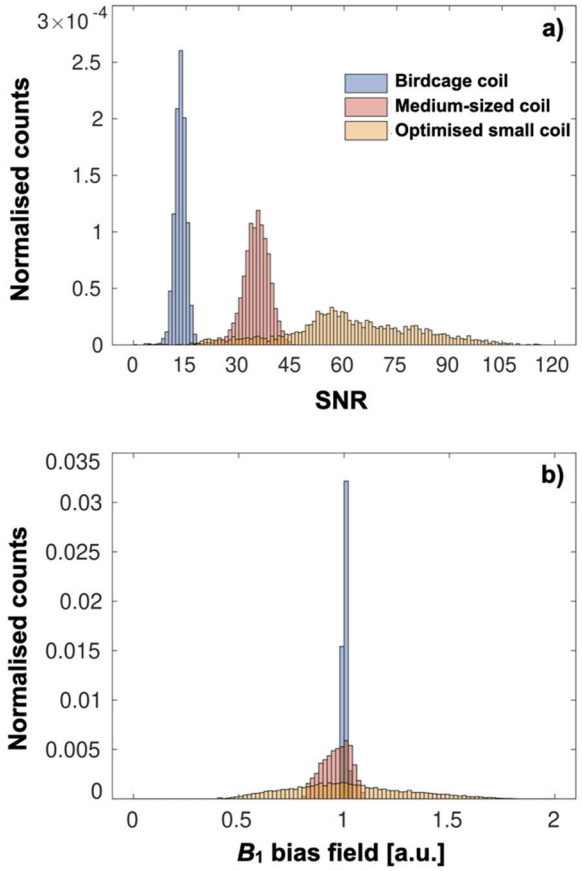

FIGURE 3. a) SNR and b) histograms of sequence-specific B_1 bias fields of the birdcage, medium-sized loop and small-sized optimised loop coils.

taurine (Tau). The SNR values for each spectrum were further obtained from the LCModel output in order to evaluate the quality of the MR spectra, in which the SNR is defined as the ratio of the maximum in the spectrum minus the baseline to twice the root-mean-square of the residuals. We also measured the relative SNR in the T_2w images in order to support the findings in the MRS analysis. Finally, the quality of the spectra was also assessed via the FWHM parameter reported by the LCModel software.

III. RESULTS

Figure 2 displays the axial, coronal and sagittal slices of the T_2w TSE images obtained using the birdcage head volume coil, the medium-sized brain loop coil and the optimised visual cortex loop coil. Their corresponding sequence-specific B_1 bias field maps can also be found at the bottom left corner in axial images. As expected, the difference in the B_1 uniformity and SNR of the individual coils is clearly noticeable.

Figure 3 shows the histogram plots of the SNR (a) and B_1 (b) of the proposed coils as estimated based on the bias field of the corresponding T_2w anatomical images. Here, the SNR value in each voxel of the optimised small-sized coil varies more significantly than the other two coils depending on the position of the voxel. The bottom of the MRS VOI (i.e. far away from the coil) in the small-sized loop coil shows lower

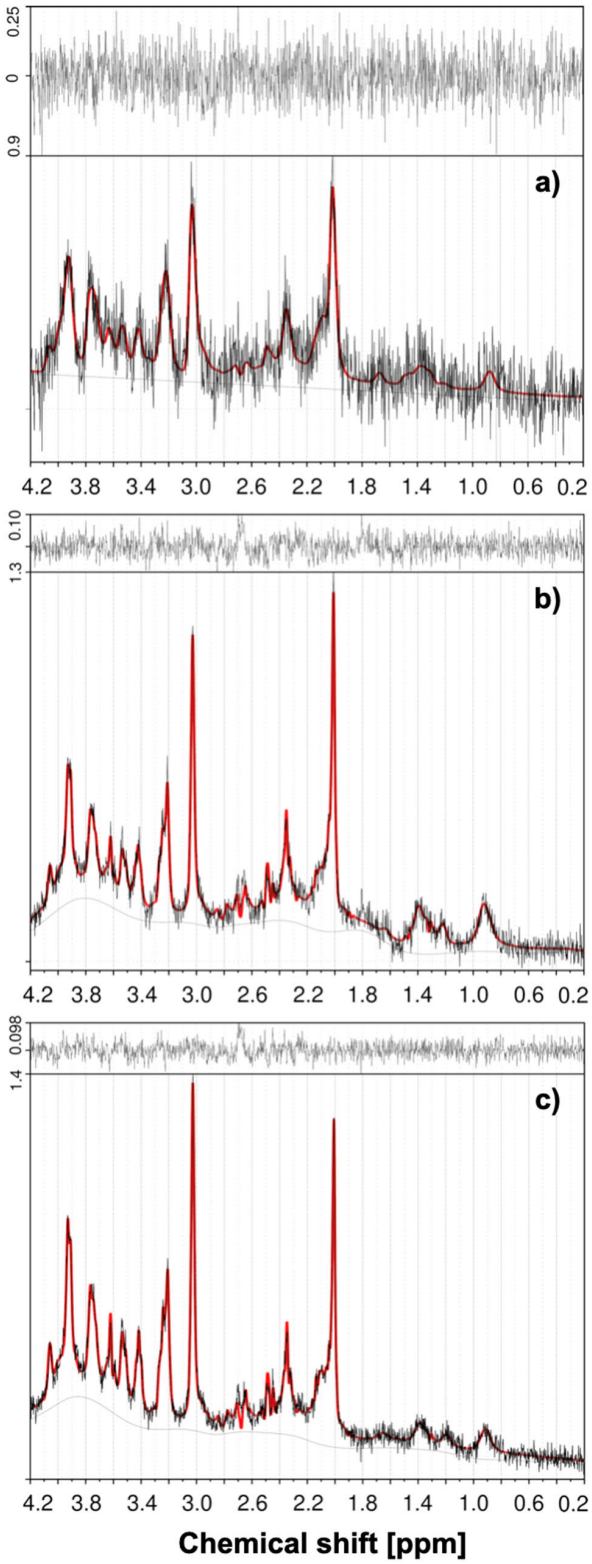

FIGURE 4. MR Spectra (solid black lines, bottom panels) obtained with the use of (a) birdcage coil, (b) medium-sized loop coil and (c) small-sized optimised loop coil with the LCModel fit (solid red lines) and the resulting residuals (top panels).

TABLE 1. Metabolite concentrations (Conc., a.u.) and Cramér-Rao lower-bound (SD, %), LCModel correlation coefficients (Corr.), FWHM and SNR values acquired using each RF coil.

	Birdcage coil		Medium-sized loop coil		Small-sized loop coil	
Metabolites	Conc. [a.u.]	SD [%]	Conc. [a.u.]	SD [%]	Conc. [a.u.]	SD [%]
Ala	2.07 *	41	0.72 *	64	-	-
Asc	3.78 *	22	1.83 *, #	21	3.58 #	9
Asp	2.09 *	51	5.93 *	13	6.03	12
GABA	0.96 *	74	2.28 *	25	1.75	29
Glc	0.52 *	117	2.16 *	20	2.47	16
Gln	5.54	29	4.48 #	18	6.13 #	11
Glu	15.20	8	13.70	4	14.30	3
GPC	0.76 *	26	1.08 *, #	6	1.21 #	5
GSH	3.85 *	13	1.36 *, #	15	2.34 #	9
Ins	6.76 *	10	5.62 *, #	5	8.62 #	3
Lac	2.66	33	1.50	37	0.80	43
NAA	10.60 *	5	9.65 *	2	9.38	2
NAAG	0.36 *	144	1.14 *	19	1.06	16
Tau	5.29	12	5.15 #	5	6.99 #	4
PE	10.90 *	15	4.56 *, #	13	6.07 #	9
tCh	0.76 *	26	1.08 *, #	6	1.21 #	5
tNAA	10.90	4	10.80	3	10.40	2
tCr	10.60 *	4	9.74 *, #	2	12.30 #	1
Glx	20.70 *	8	18.10 *, #	5	20.40 #	4
Corr. Cr-PCr	-0.89		-0.88		-0.88	
Corr. Gln-Glu	-0.36		0.09		0.12	
Corr. NAA-NAAG	-0.60		-0.15		-0.11	
$FWHM_{wr}$	25.1		14.8		13.4	
$FWHM_{spec}$	17.6		6.8		6.0	
SNR_{wr}	158		720		943	
SNR_{spec}	5		17		23	
SNR_{T2w}	13 ± 2		35 ± 4		62 ± 19	

Note: Significant differences between concentrations within one SD for the birdcage coil versus the medium-sized loop coil are denoted with the symbol (*), whereas it is denoted with the symbol (#) for the medium-sized loop coil versus the small-sized loop coil. The middle section shows the LCModel correlation coefficients between typical metabolite pairs. The last table section shows the SNR and FWHM (Hz) for each coil. Subscripts wr and spec at the bottom of this table refer to the water reference and spectrum, respectively.

SNR within the coil, although the SNR value is still higher than or as high as that from the birdcage or medium-sized coils. The same behaviour is observed in the B_1 histogram plots.

Figure 4 shows the MRS spectra (solid black lines) acquired using different coils: a) birdcage, b) medium-sized loop and c) small-sized loop. In addition, the LCModel fits (solid red lines) and the resulting residuals (top panels) are also shown.

The SNR improvement of the medium loop coil, when compared to the birdcage coil shown in Figure 2, clearly leads a substantial reduction in the fitting residuals and, therefore, an increase in the LCModel SNR values. This finding is also shown in Figures 3a and 4b and Table 1. For the case of the optimised small loop coil, the SNR increase shown in Figure 2 is subtler, although this increase is also observable in a further reduction of the residuals, shown in Figure 4c. The SNR increase from the birdcage coil to the medium loop coil also resulted in a reduction of the FWHM of the spectra, from 17.6 Hz to 6.8 Hz. This improvement, although smaller (from 6.8 to 6 Hz), was also found when comparing the FWHM of the medium loop with that of the small loop coil.

Table 1 shows the metabolite concentrations obtained with the LCModel. Since neither PCh nor Ala was detected by any of the coils, these metabolites were excluded from further consideration. Other metabolites (e.g. Glc and NAAG for the birdcage coil) were detected but showed exceedingly large Cramér-Rao lower-bound (SD) values (> 100%). However, these were included in Table 1 for the sake of assessing the improvement as a result of the increased SNR. Nevertheless, assuming a threshold for SD equal to 30% for a reliable quantification (typical value in literature [33]), the following metabolites were not reliably detected: Ala, Asp, GABA, Glc, Lac and NAAG (for birdcage); Ala and Lac (for medium and

small loop). Moreover, given the strong negative correlation between Cr and PCr (Table 1, middle row segment), we only report the total concentration (i.e. tCr), as typically used in the literature [34].

Table 1 also shows that the SD values of the metabolites Asp, GABA, Glc, Gln, Glu, GPC, Ins, NAA, NAAG, Tau, tCh, tNAA, tCr and Glx improved by a factor ∼4 for the medium loop coil compared to the birdcage coil. Only the SD for Ala, Asc, GSH, Lac and PE remained approximately the same or slightly increased for the medium loop compared to the birdcage. Metabolites with improved SD (factor ∼4) for the small loop compared to the medium loop coil were: Asc, Gln, GSH, Ins, tNAA and tCr. For the rest of the metabolites, SD either stayed at a nearly identical level or slightly increased. Table 1 also shows that the correlation of Cr and PCr did not improve with increasing SNR, as previously observed [35]. Conversely, the correlation coefficient for the metabolite pairs Gln-Glu and NAA-NAAG did show improvements with increasing SNR.

Furthermore, based on the assumption that two metabolite concentrations are significantly different if they differ by more than the sum of their corresponding SDs, then Glu, Gln, Lac, Tau and tNAA were not significantly different between the birdcage coil and the medium loop coil. This was also the case for Asp, GABA, Glc, Glu, Lac, NAA, NAAG and tNAA between the medium loop and the small loop. The latter suggests that the metabolic profile tends to be more reproducible between the medium loop and small loop coil compared to the birdcage coil.

IV. DISCUSSION

Since preclinical single-voxel ^{1}H-MRS records the metabolite signals from a small and restricted VOI to prevent signal contamination from other regions, an intrinsically low SNR is inevitable due to the reduction of proportionally detectable MR signal levels. Consequently, one of the principal challenges is to acquire MR spectra with sufficient SNR, which substantially determines the practical constraint to the size of the VOI and the acquisition time. In order to increase the sensitivity, it is possible to average the data a large number of times within the given measurement time. However, in some cases, even a large number of averages does not suffice to achieve high enough SNR values within the given acquisition time. For preclinical studies, large groups of animals are often scanned, which can, in turn, lead to an unacceptably long project duration. In some cases, it is mandatory that the animals are monitored more than once in a longitudinal manner and are weak due to the implemented disease models. Thus, it is crucial to design experimental setups that maximise the SNR values within the shortest possible acquisition time, for which several means can be proposed.

The most intuitive solution to improve SNR - but coming at a high expense - is to simply increase the main static magnetic field strength (B_0) of the MR scanner to ultra- or even extremely-high field strengths, as the SNR increase is nearly supralinear to that of the magnetic field [36]. Therefore, most small animal experiments tend to be performed at ultra-high field (> 7 T). Tailoring MR pulse sequences for a target metabolite should also help to support the SNR improvement and investigation of the specific metabolite, for example, using the MEGA-PRESS sequence for GABA measurements [37]. As demonstrated in this study, customising the RF coil according to its size and target region of interest can also be another significant means of gaining SNR. The size of the coil is inversely proportional to the sensitivity but proportional to the penetration depth, i.e. smaller coils provide higher SNR with less coverage. In our comparison, the SNR measured using the optimised small loop coil appeared to be approximately 5 and 1.35 times higher than that measured using the birdcage volume head coil and the medium CP loop coil, respectively. In other words, the acquisition can be completed 25 and 1.8 times quicker, or alternatively, much higher resolution can be achieved within the same measurement time. Importantly, all the coils fully covered the desired voxel in the visual cortex.

This optimised setup with improved SNR could be applied to investigations of the visual cortex or other cortical regions (motor or auditory cortex) using single-voxel MRS, in similar MRS and MRI studies in humans [38], [39], [40], [41] or in microscopic MR imaging [42], [43]. Depending on the depth of the target voxel, slight adjustments of the coil dimensions might result in even better SNR values.

Although SNR could be further improved by building smaller RF coils than the ones shown in this work, smaller coils would reduce the coverage and RF homogeneity, especially for bigger rats. In addition, it would be difficult to handle the construction of small loops with relatively larger coil components, such as capacitors and trimmers. We also found that due to its reduced coverage, the reproducibility in the coil positioning was more difficult for the smaller coil. Despite being practically difficult due to the requirement of more components in such a limited space, this work could also certainly be extended to combine multi-channel receive (Rx) only phased array coils together with a smaller transmit (Tx) only coil. This combination was not included this time due to the reasons outlined relating to the space and due to the fact that our current Tx coil is not able to provide sufficient power to the excitation pulse and water suppression. Nevertheless, in principle, using multi-channel Rx arrays may also be advantageous in MRS since a more homogeneous Tx field and highly sensitive Rx signal might be achieved [44]. If practically feasible, using implanted micro-coils [45], [46], [47] and cryocooled coils [48], [49], [50], [51], [52] would also be beneficial to enhance SNR in very small and specific areas.

In general, a coil benchmarking may have to be carried out when a coil is newly developed [53], [54], [55] or when the performance of a double-tuned or MR-PET hybrid coil is compared against its counterpart single-tuned or single-modality coil [56], [57]. In this study, we built three coils with different coil types and geometries, and each coil was built to focus on the coverage of a different target. Comparing

these coils provides information and allows them to be benchmarked against each other.

Concomitant with the increase in SNR values for the case of smaller optimised loop coils is the reduction in B_1 homogeneity as shown in Figure 3b. This feature can drastically affect the image bias, as observed in this work for the case of T_2w anatomical images and maps in Figure 2 and the plots in Figure 3a. Hence, if image homogeneity is the main concern in a given experiment, then larger loops or volume coils would be preferential to smaller optimised loops. In the context of MRS, however, this limitation can be easily mitigated by using B_1 insensitive MRS pulse sequences, such as the LASER sequence, together with the VAPOR water saturation scheme used in this work [24], [25]. Indeed, the LASER sequence utilised in our work is composed of different modules which are designed to be highly insensitive to B_1 inhomogeneity. Firstly, the VAPOR module is used to decrease the sensitivity to the applied RF power and has been demonstrated to suppress the water signal even in the case of highly inhomogeneous B_1 fields, such as for a surface coil [58]. In particular, Tkáč et al. reported a residual water signal of less than 5% for a range of flip angles between 40° and 160° [58]. Secondly, excitation and volume selection in LASER are performed using fully adiabatic RF pulses, namely a non-selective adiabatic half-passage pulse for excitation and three pairs of adiabatic full passage pulses in each dimension for volume selection. In the current implementation, hyperbolic secant pulses were used [23], [24]. The use of such adiabatic RF pulses has been shown to provide spectra highly insensitive to the B_1 inhomogeneity [22], [23].

In terms of B_0 shimming, although all of the coils were built using non-magnetic components, the position of these components differs from each coil, which may vary the required shim values. However, the effect on shimming is determined by the inserted sample (i.e. the rat) and the different arrangements did not cause any problem. We also performed the B_0 shimming using the FASTESTMAP method using the same procedure for all the measurements, namely via monitoring the FWHM while we calibrated the values prior to the MRS acquisition.

In this study, multiple measurements with different animals were not conducted, and statistical analysis could not be performed since the effect from the single animal was significant and agreed well with the previous well-known work [16].

V. CONCLUSION

We have demonstrated a project-oriented RF coil design optimisation that is effective and relatively simple to build. As this study focussed on the visual cortex, new optimisation would be required if the studies, for example, focus on the investigation of other or deeper brain regions. In conclusion, although the default coil setting provided by manufacturers is advantageous when whole brain or whole head coverage is required, it could be limiting in certain studies, one example of which has been shown here. By using an optimised setup, we can either significantly reduce the entire measurement time or acquire MR images or spectra with much improved SNR or higher resolution. This also gives more precise measurements with a minimum error and time to include additional, potentially interesting, sequences for multi-parametric studies or multiple voxel comparisons. Moreover, the shortened scan time both supports animal welfare and enables more animals to be scanned within the given measurement time.

ACKNOWLEDGMENT

The authors would like to thank E. J. Auerbach and M. Marjanska (Centre for Magnetic Resonance Research and the Department of Radiology, University of Minnesota, USA) for the development of the LASER and FASTESTMAP sequences for the Siemens platform, which was provided by the University of Minnesota under a C2P agreement and also would like to thank Claire Rick for English proofreading.

REFERENCES

[1] S. V. Ovsepian, I. Olefir, G. Westmeyer, D. Razansky, and V. Ntziachristos, "Pushing the boundaries of neuroimaging with optoacoustics," *Neuron*, vol. 96, no. 5, pp. 966–988, Dec. 2017.

[2] A. I. Silva, J. E. Haddon, Y. Ahmed Syed, S. Trent, T.-C.-E. Lin, Y. Patel, J. Carter, N. Haan, R. C. Honey, T. Humby, Y. Assaf, M. J. Owen, D. E. J. Linden, J. Hall, and L. S. Wilkinson, "Cyfip1 haploinsufficient rats show white matter changes, myelin thinning, abnormal oligodendrocytes and behavioural inflexibility," *Nature Commun.*, vol. 10, no. 1, p. 3455, Aug. 2019.

[3] F. Rizzo, A. Abaei, E. Nespoli, J. M. Fegert, B. Hengerer, V. Rasche, and T. M. Boeckers, "Aripiprazole and riluzole treatment alters behavior and neurometabolites in young ADHD rats: A longitudinal 1H-NMR spectroscopy study at 11.7T," *Translational Psychiatry*, vol. 7, no. 8, pp. e1189–e1189, Aug. 2017.

[4] C. Hoyer, N. Gass, W. Weber-Fahr, and A. Sartorius, "Advantages and challenges of small animal magnetic resonance imaging as a translational tool," *Neuropsychobiology*, vol. 69, no. 4, pp. 187–201, 2014.

[5] L.-M. Hsu, X. Liang, H. Gu, J. K. Brynildsen, J. A. Stark, J. A. Ash, C.-P. Lin, H. Lu, P. R. Rapp, E. A. Stein, and Y. Yang, "Constituents and functional implications of the rat default mode network," *Proc. Nat. Acad. Sci. USA*, vol. 113, no. 31, pp. E4541–E4547, Aug. 2016.

[6] K. C. Chan, K.-F. So, and E. X. Wu, "Proton magnetic resonance spectroscopy revealed choline reduction in the visual cortex in an experimental model of chronic glaucoma," *Experim. Eye Res.*, vol. 88, no. 1, pp. 65–70, Jan. 2009.

[7] F. Duan, Z. Xiao, Y. Wang, X. Sun, Z. Tang, R. Wang, L. Guo, W. Tang, T. Liu, P. Wang, and Y. Zhan, "Metabolic alterations in the visual pathway of retinitis pigmentosa rats: A longitudinal multimodal magnetic resonance imaging study with histopathological validation," *NMR Biomed.*, vol. 35, no. 9, p. e4751, Sep. 2022.

[8] T. Plank, E. M. A. Benkowitsch, A. L. Beer, S. Brandl, M. Malania, S. M. Frank, H. Jägle, and M. W. Greenlee, "Cortical thickness related to compensatory viewing strategies in patients with macular degeneration," *Frontiers Neurosci.*, vol. 15, Oct. 2021, Art. no. 718737.

[9] S. Li, X. Wang, J. Yang, H. Lei, X. Wang, and Y. Xiang, "Metabolic profile of visual cortex in diabetic rats measured with in vivo proton MRS," *NMR Biomed.*, vol. 30, no. 11, p. e3783, Nov. 2017.

[10] T. Ishihara, T. Ozawa, M. Otsuki, J. Shimbo, K. Tanaka, and M. Nishizawa, "Atypical micrographia associated with corticostriatal white matter lesions in systemic lupus erythematosus," *J. Neurol., Neurosurgery Psychiatry*, vol. 77, pp. 4–993, Aug. 2006.

[11] C. Lunghi, "Visual cortex rewiring in retinitis pigmentosa: Plasticity is preserved," *Neuroscience*, vol. 424, pp. 203–204, Jan. 2020.

[12] P. B. Barker, D. O. Hearshen, and M. D. Boska, "Single-voxel proton MRS of the human brain at 1.5T and 3.0T," *Magn. Reson. Med.*, vol. 45, pp. 765–769, May 2001.

[13] G. Öz, "Advanced single voxel 1 h magnetic resonance spectroscopy techniques in humans: Experts' consensus recommendations," *NMR Biomed.*, vol. 34, no. 5, p. e4236, May 2021.

[14] H. H. Zhu and P. B. Barker, "MR spectroscopy and spectroscopic imaging of the brain," *Methods Mol. Biol.*, vol. 711, pp. 203–226, Aug. 2011.

[15] B. Lanz, "Magnetic resonance spectroscopy in the rodent brain: Experts' consensus recommendations," *NMR Biomed.*, vol. 26, p. e4325, Aug. 2020.

[16] D. I. Hoult and R. E. Richards, "The signal-to-noise ratio of the nuclear magnetic resonance experiment," *J. Magn. Reson.*, vol. 24, no. 1, pp. 71–85, Oct. 1976.

[17] P. B. Roemer, W. A. Edelstein, C. E. Hayes, S. P. Souza, and O. M. Mueller, "The NMR phased array," *Magn. Reson. Med.*, vol. 16, no. 2, pp. 192–225, 1990.

[18] C.-H. Choi, Y. Ha, P. Veeraiah, J. Felder, K. Möllenhoff, and N. J. Shah, "Design and implementation of a simple multinuclear MRI system for ultra high-field imaging of animals," *J. Magn. Reson.*, vol. 273, pp. 28–32, Dec. 2016.

[19] J. Felder, A. A. Celik, C.-H. Choi, S. Schwan, and N. J. Shah, "9.4 T small animal MRI using clinical components for direct translational studies," *J. Translational Med.*, vol. 15, no. 1, p. 264, Dec. 2017.

[20] J. Hennig, A. Nauerth, and H. Friedburg, "RARE imaging: A fast imaging method for clinical MR," *Magn. Reson. Med.*, vol. 3, pp. 33–823, Dec. 1986.

[21] R. Gruetter and I. Tkac, "Field mapping without reference scan using asymmetric echo-planar techniques," *Magn. Reson. Med.*, vol. 43, pp. 23–319, Feb. 2000.

[22] I. Tkac, Z. Starc, I. Choi, and R. Gruetter, "In Vivo 1H NMR spectroscopy of rat brain at 1 ms echo time," *Magn. Reson. Med.*, vol. 41, pp. 56–649, Apr. 1999.

[23] M. Garwood and L. DelaBarre, "The return of the frequency sweep: Designing adiabatic pulses for contemporary NMR," *J. Magn. Reson.*, vol. 153, no. 2, pp. 155–177, Dec. 2001.

[24] R. L. Muetzel, P. F. Collins, M. P. Becker, R. Valabrègue, E. J. Auerbach, K. O. Lim, and M. Luciana, "In vivo 1H magnetic resonance spectroscopy in young-adult daily marijuana users," *NeuroImage, Clin.*, vol. 2, pp. 581–589, Apr. 2013.

[25] N. Allaïli, R. Valabrègue, E. J. Auerbach, V. Guillemot, L. Yahia-Cherif, E. Bardinet, M. Jabourian, P. Fossati, S. Lehéricy, and M. Marjanska, "Single-voxel1H spectroscopy in the human hippocampus at 3 T using the LASER sequence: Characterization of neurochemical profile and reproducibility," *NMR Biomed.*, vol. 28, no. 10, pp. 1209–1217, Oct. 2015.

[26] Y. Zhang, M. Brady, and S. Smith, "Segmentation of brain MR images through a hidden Markov random field model and the expectation-maximization algorithm," *IEEE Trans. Med. Imag.*, vol. 20, no. 1, pp. 45–57, Jan. 2001.

[27] R. Simpson, G. A. Devenyi, P. Jezzard, T. J. Hennessy, and J. Near, "Advanced processing and simulation of MRS data using the FID appliance (FID-A)—An open source, MATLAB-based toolkit," *Magn. Reson. Med.*, vol. 77, no. 1, pp. 23–33, Jan. 2017.

[28] J. Near, R. Edden, C. J. Evans, R. Paquin, A. Harris, and P. Jezzard, "Frequency and phase drift correction of magnetic resonance spectroscopy data by spectral registration in the time domain," *Magn. Reson. Med.*, vol. 73, no. 1, pp. 44–50, Jan. 2015.

[29] S. W. Provencher, "Estimation of metabolite concentrations from localized in vivo proton NMR spectra," *Magn. Reson. Med.*, vol. 30, pp. 9–672, Dec. 1993.

[30] P. G. Henry, M. Marjanska, J. D. Walls, J. Valette, R. Gruetter, and K. Ugurbil, "Proton-observed carbon-edited NMR spectroscopy in strongly coupled second-order spin systems," *Magn. Reson. Med.*, vol. 55, pp. 7–250, Feb. 2006.

[31] V. Govindaraju, K. Young, and A. A. Maudsley, "Corrigendum: Proton NMR chemical shifts and coupling constants for brain metabolites," *NMR Biomed.*, vol. 28, pp. 4–923, Jul. 2015.

[32] V. Govindaraju, K. Young, and A. A. Maudsley, "Proton NMR chemical shifts and coupling constants for brain metabolites," *NMR Biomed.*, vol. 13, pp. 53–129, May 2000.

[33] J. Near, A. D. Harris, C. Juchem, R. Kreis, M. Marjanska, G. Öz, J. Slotboom, M. Wilson, and C. Gasparovic, "Preprocessing, analysis and quantification in single-voxel magnetic resonance spectroscopy: Experts' consensus recommendations," *NMR Biomed.*, vol. 34, no. 5, p. e4257, May 2021.

[34] D. K. Deelchand, I. M. Adanyeguh, U. E. Emir, T. M. Nguyen, R. Valabregue, P. G. Henry, F. Mochel, and G. Oz, "Two-site reproducibility of cerebellar and brainstem neurochemical profiles with short-echo, single-voxel MRS at 3T," *Magn. Reson. Med.*, vol. 73, pp. 25–1718, May 2015.

[35] I. Tkac, G. Oz, G. Adriany, K. Uğurbil, and R. Gruetter, "In vivo 1H NMR spectroscopy of the human brain at high magnetic fields: Metabolite quantification at 4T vs. 7T," *Magn. Reson. Med.*, vol. 62, pp. 868–879, Oct. 2009.

[36] R. Pohmann, O. Speck, and K. Scheffler, "Signal-to-noise ratio and MR tissue parameters in human brain imaging at 3, 7, and 9.4 Tesla using current receive coil arrays," *Magn. Reson. Med.*, vol. 75, pp. 9–801, Feb. 2016.

[37] M. Mescher, H. Merkle, J. Kirsch, M. Garwood, and R. Gruetter, "Simultaneous in vivo spectral editing and water suppression," *NMR Biomed.*, vol. 11, pp. 72–266, Oct. 1998.

[38] S. Mangia, "Sensitivity of single-voxel 1H-MRS in investigating the metabolism of the activated human visual cortex at 7 T," *Magn. Reson. Imag.*, vol. 24, pp. 343–348, May 2006.

[39] J. A. Stanley and N. Raz, "Functional magnetic resonance spectroscopy: The 'new' MRS for cognitive neuroscience and psychiatry research," *Front Psychiatry*, vol. 9, p. 76, Mar. 2018.

[40] C. Ligneul, F. F. Fernandes, and N. Shemesh, "High temporal resolution functional magnetic resonance spectroscopy in the mouse upon visual stimulation," *NeuroImage*, vol. 234, Jul. 2021, Art. no. 117973.

[41] H.-S. Kim, B.-P. Song, R. Kim, W.-C. Choi, D. Kim, W. M. Shim, K.-N. Kim, and S.-K. Lee, "Customized radiofrequency phased-array coil combining transmit-only, receive-only, and transmit/receive coils for magnetic resonance imaging of visual cortex at 7 Tesla," *IEEE Access*, vol. 10, pp. 42097–42107, 2022.

[42] B. Driehuys, J. Nouls, A. Badea, E. Bucholz, K. Ghaghada, A. Petiet, and L. W. Hedlund, "Small animal imaging with magnetic resonance microscopy," *ILAR J.*, vol. 49, no. 1, pp. 35–53, Jan. 2008.

[43] A. Alkemade, P.-L. Bazin, R. Balesar, K. Pine, E. Kirilina, H. E. Möller, R. Trampel, J. M. Kros, M. C. Keuken, R. L. A. W. Bleys, D. F. Swaab, A. Herrler, N. Weiskopf, and B. U. Forstmann, "A unified 3D map of microscopic architecture and MRI of the human brain," *Sci. Adv.*, vol. 8, no. 17, Apr. 2022, Art. no. eabj7892.

[44] F. Du, N. Li, X. Yang, B. Zhang, X. Zhang, and Y. Li, "Design and construction of an 8-channel transceiver coil array for rat imaging at 9.4 T," *J. Magn. Reson.*, vol. 351, Jun. 2023, Art. no. 107302, doi: 10.1016/j.jmr.2022.107302.

[45] A. G. Webb, "Radiofrequency microcoils for magnetic resonance imaging and spectroscopy," *J. Magn. Reson.*, vol. 229, pp. 55–66, Apr. 2013.

[46] J. Deborne, N. Pinaud, and Y. Crémillieux, "Proton MRS on sub-microliter volume in rat brain using implantable NMR microcoils," *NMR Biomed.*, vol. 34, no. 10, p. e4578, Oct. 2021.

[47] J. Deborne, N. Pinaud, and Y. Crémillieux, "Implantable NMR microcoils in rats: A new tool for exploring tumor metabolism at sub-microliter scale?" *Metabolites*, vol. 11, no. 3, p. 176, Mar. 2021.

[48] C. Baltes, N. Radzwill, S. Bosshard, D. Marek, and M. Rudin, "Micro MRI of the mouse brain using a novel 400 MHz cryogenic quadrature RF probe," *NMR Biomed.*, vol. 22, pp. 42–834, Oct. 2009.

[49] C. Koo, R. F. Godley, M. P. McDougall, S. M. Wright, and A. Han, "A microfluidically cryocooled spiral microcoil with inductive coupling for MR microscopy," *IEEE Trans. Biomed. Eng.*, vol. 61, no. 1, pp. 76–84, Jan. 2014.

[50] J. D. Sánchez-Heredia, R. Baron, E. S. S. Hansen, C. Laustsen, V. Zhurbenko, and J. H. Ardenkjr-Larsen, "Autonomous cryogenic RF receive coil for 13 C imaging of rodents at 3 T," *Magn. Reson. Med.*, vol. 84, no. 1, pp. 497–508, Jul. 2020.

[51] A. Arbabi, L. S. Noakes, D. Vousden, J. Dazai, S. Spring, O. Botelho, T. Keshavarzian, M. Mattingly, J. E. Ellegood, L. M. J. Nutter, R. Wissmann, J. G. Sled, J. P. Lerch, R. M. Henkelman, and B. J. Nieman, "Multiple-mouse magnetic resonance imaging with cryogenic radiofrequency probes for evaluation of brain development," *NeuroImage*, vol. 252, May 2022, Art. no. 119008.

[52] T. Niendorf, A. Pohlmann, H. M. Reimann, H. Waiczies, E. Peper, T. Huelnhagen, E. Seeliger, A. Schreiber, R. Kettritz, K. Strobel, M.-C. Ku, and S. Waiczies, "Advancing cardiovascular, neurovascular, and renal magnetic resonance imaging in small rodents using cryogenic radiofrequency coil technology," *Frontiers Pharmacol.*, vol. 6, p. 255, Nov. 2015.

[53] M. M. Garcia, T. R. Oliveira, D. Papoti, K. T. Chaim, M. C. G. Otaduy, D. Erni, and W. Zylka, "Experimental and numerical investigations of a small animal coil for ultra-high field magnetic resonance imaging (7T)," *Current Directions Biomed. Eng.*, vol. 5, no. 1, pp. 525–528, Sep. 2019.
[54] O. Weinberger, L. Winter, M. A. Dieringer, A. Els, C. Oezerdem, J. Rieger, A. Kuehne, A. M. Cassara, H. Pfeiffer, F. Wetterling, and T. Niendorf, "Local multi-channel RF surface coil versus body RF coil transmission for cardiac magnetic resonance at 3 Tesla: Which configuration is winning the game?" *PLoS ONE*, vol. 11, no. 9, Sep. 2016, Art. no. e0161863.
[55] T. Feuillet, M.-J. Seurin, O. Leveneur, E. Viguier, and O. Beuf, "Coil optimization for low-field MRI: A dedicated process for small animal preclinical studies," *Lab Animals*, vol. 49, no. 2, pp. 153–167, Apr. 2015.
[56] Y. Ha, C. Choi, and N. J. Shah, "Development and implementation of a PIN-diode controlled, quadrature-enhanced, double-tuned RF coil for sodium MRI," *IEEE Trans. Med. Imag.*, vol. 37, no. 7, pp. 1626–1631, Jul. 2018.
[57] C.-H. Choi, T. Felder, J. Felder, L. Tellmann, S.-M. Hong, H.-P. Wegener, N. J. Shah, and K. Ziemons, "Design, evaluation and comparison of endorectal coils for hybrid MR-PET imaging of the prostate," *Phys. Med. Biol.*, vol. 65, no. 11, Jun. 2020, Art. no. 115005.
[58] I. Tkáć, Z. Starčuk, I.-Y. Choi, and R. Gruetter, "In vivo1H NMR spectroscopy of rat brain at 1 ms echo time," *Magn. Reson. Med.*, vol. 41, no. 4, pp. 649–656, Apr. 1999.

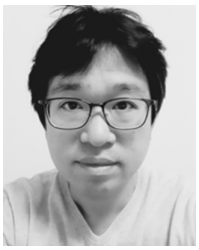

CHANG-HOON CHOI received the Ph.D. degree in MRI physics from the University of Aberdeen, Aberdeen, U.K., in 2010. He was with MR Solutions Ltd., Guildford, U.K., until 2014. He is currently a MR expert and has been a Senior Scientist with Forschungszentrum Juelich, Germany, since 2014.

EZEQUIEL FARRHER received the degree in physics from the National University of Córdoba, Argentina, in 2008, and the Ph.D. degree in MRI physics from RWTH Aachen University, Germany, in 2013. He is currently a Senior Scientist with Forschungszentrum Juelich, Germany.

JÖRG FELDER (Senior Member, IEEE) received the Diploma degree in electrical engineering and the Ph.D. degree from RWTH Aachen University, Aachen, Germany, in 1998 and 2004, respectively. From 2004 to 2007, he was a RF Engineer with Bruker BioSpin MRI GmbH, Ettlingen, Germany. Since 2007, he has been a Team Leader with Forschungszentrum Juelich, Germany.

JING WANG received the master's degree in ophthalmology from Sun Yat-sen University, Guangzhou, China, in 2014, and the Ph.D. degree in neuroscience, in April 2021. She was a Resident Physician with the Zhongshan Ophthalmic Centre, Guangzhou, China, until 2016. Since 2019, she has been an attending physician in ophthalmology.

ANTJE WILLUWEIT received the Ph.D. degree in biology from the University of Darmstadt, Germany, in 2000. She worked in several biotech companies, before she joined Forschungszentrum Juelich, Germany, in 2011. She is currently a team leader and an expert in laboratory animals modeling human diseases.

N. JON SHAH received the Ph.D. degree from The University of Manchester, U.K. He worked on the development of methods for MRI and spectroscopy in Japan. He was with the University of Cambridge, U.K., on MR and then in Germany, where he is currently with Forschungszentrum Juelich. He is also the Director of the Institute of Neuroscience and Medicine—4 and the Institute of Neuroscience and Medicine—11, Juelich, and a Professor in MRI physics with RWTH, Aachen, Germany.